Anomalous Hall conductivity and quantum friction

Pavel Středa and Karel Výborný
Institute of Physics, Academy of Sciences of the Czech Republic, Cukrovarnická 10, 16253 Praha 6, Czech Republic

(Received 27 July 2022; revised 31 October 2022; accepted 30 November 2022; published xxxxxxxxxx)

The anomalous Hall effect in high conductivity region is studied using a two-dimensional network model. We find that the off-diagonal conductivity comprises two parts: one which reflects the bulk properties as obtained by the Kubo formula and another which is sensitive to boundary conditions imposed on the network. In the fully coherent limit, the latter scales with the width of the conducting channel, while for real-world samples, it is controlled by the coherence length. It provides an alternative interpretation of the observed behavior in the clean limit which is otherwise attributed to the skew scattering. We highlight analogies to friction in viscous fluids responsible for Couette flow. In the present case, this quantum effect is governed by wave interference.

DOI: 10.1103/PhysRevB.00.004400

I. INTRODUCTION

Scattering is an essential ingredient to many transport phenomena. The anomalous Hall conductivity $\sigma_{\rm AH}$ of ferromagnetic systems provides a notable exception to this rule but only in certain region: most materials with *moderate* longitudinal conductivity σ_0 show almost constant $\sigma_{\rm AH}$ as scattering strength and hence σ_0 is varied. This property seems to be well understood in terms of the Berry curvature of occupied electronic bands representing properties of ideal Bloch systems, also called the intrinsic region of the anomalous Hall effect (AHE). This interval of roughly 10^4 to 10^6 inverse $\Omega\,$cm is surrounded by regions in which $\sigma_{\rm AH}(\sigma_0)$ becomes scattering dependent as reviewed by Nagaosa *et al.* [1]. While suppression of $\sigma_{\rm AH}$ for stronger disorder is natural, its linear increase with σ_0 in high conductivity regions [2] is, at least, surprising. It is generally accepted that it is caused by skew scattering [3–7], asymmetric scattering of electrons on impurities induced by their nonzero spin. Its effect increases with decreasing impurity concentration. A seemingly inevitable consequence of this argumentation is that anomalous Hall conductivity in clean systems is driven by negligible impurity concentration while in this limit intrinsic values obtained for ideal Bloch systems could be expected. With few notable exceptions, the effect of Berry phases [see Eq. (4) below] is ignored in the context of skew scattering and even if it is not [8], the lack of generality [see Eq. (A7) in Appendix] leads to the contradiction mentioned above. The main aim of the present treatment is to suggest another possible origin of the observed increase of the Hall conductivity with sample purity which does not rely on skew scattering.

Basic condition for the observation of AHE in magnetic systems is the existence of nonzero orbital momentum [9], which can be induced by spin-orbit interaction or noncoplanar magnetic order [10]. It is responsible for the violation of time reversal symmetry, a necessary condition for nonzero Hall effect. Transport properties are measured on stripes, Hall bar samples, and orbital momentum of atomic-type wave functions causes the space current density oscillating across the stripe. It can be represented by current paths with alternating current directions [11]. Physically acceptable paths at edges should be of the chiral type leading current along opposite directions and the total net current thus vanishes in the equilibrium. Voltage drop applied between stripe edges induces changes of the electron concentrations within current paths. It leads to the polarization of the system which is a typical property accompanying the anomalous Hall effect [12–14]. Coupling between current paths is generally represented by their mutual friction. It defines momentum transfer between edges as well as Hall current through the stripe cross section. In quantum coherent systems such friction is controlled by the wave interference. The main aim of our approach to AHE is to show that quantum friction [15] between chiral current paths can be responsible for a linear increase of the anomalous Hall conductivity with σ_0 in the high conductivity region. It is an extrinsic contribution due to the finite sample dimensions.

To verify this idea, a two-dimensional network model [16] will be used. It allows to apply theory of quantum graphs [17] ideally suited for studies of interference effects. It contains all basic ingredients necessary for the existence of AHE. Coupling between atomic orbitals is defined by S matrix, which is convenient for application of the scattering matrix approach invented by Landauer [18]. Detailed model description and its basic properties are presented in Sec. II. The subsequent section is devoted to the properties of edge states. It will be shown that chiral edge states crossing energy gaps which are responsible for the quantum Hall effect [19] can be created or removed by tuning the boundary conditions. Contrary to the case of external rational magnetic fields [20], chirality is not determined by wave function properties at the Brillouin zone boundaries. The key part of our treatment is described in Sec. IV where scattering matrix approach is applied to obtain intrinsic Hall conductivity and enhanced Hall current given by friction between chiral current paths. In Sec. V, a brief summary of experimental works on anomalous Hall conductivity

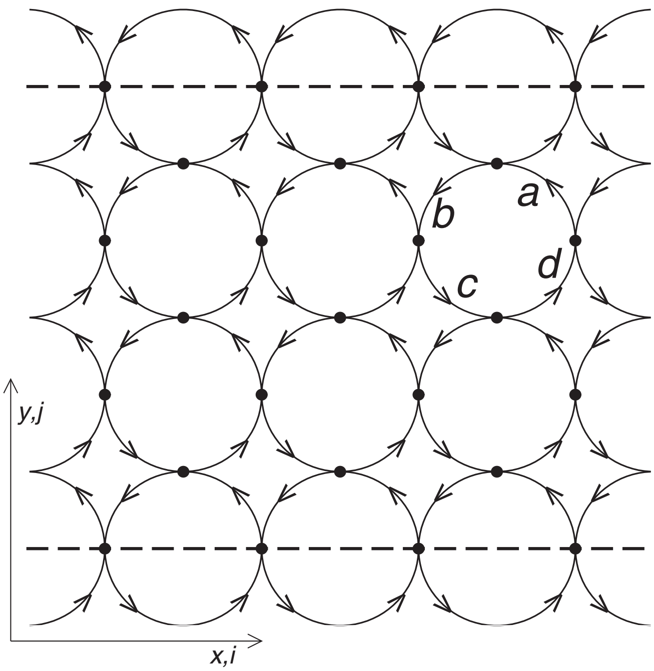

FIG. 1. Two-dimensional network model of coupled orbitals with positive orbital momenta controlled by parameter δ. Arrows are indicating direction of the electron motion and ϕ range of amplitudes a, b, c, d is defined in Table I.

in all three regions is given and a two band model is used to obtain its qualitative features for a large range of the system disorder strength. It is shown that the experimentally observed behavior of $\sigma_{\rm AH}(\sigma_0)$ can be reproduced without invoking the skew scattering mechanism. The paper will be completed by summary of main results and concluding remarks.

II. TWO-DIMENSIONAL NETWORK MODEL

In strictly two-dimensional systems, spin-orbit interaction having form $L_z s_z$, L_z being orbital momentum, separates electrons into two independent groups having spin $s_z = 1/2$ and $-1/2$, respectively. Atomic state of the orbital number m and spin s_z has the same energy as that with $-m$ and $-s_z$. Degeneracy of corresponding bands is removed by exchange interaction which will be approximated by an effective Zeeman splitting. To estimate general features of the anomalous conductivity, the simple two-dimensional network model sketched in Fig. 1 has been used [16]. It allows to employ theory of graphs [17] for single-mode quantum structure with δ-type coupling between orbitals [21]. Such type of model graphs (e.g., Chalker-Coddington model [22]) has already been applied to describe localization effect in quantum Hall systems [23] and properties of quantum spin-Hall systems [24].

TABLE I. Definition of a, b, c, d for piecewise constant $A(\phi)$ pertaining to the ring at $\vec{R}_{i,j}$.

amplitude	for $\phi \in$
$a_{i,j}$	$(0, \pi/2)$
$b_{i,j}$	$(\pi/2, \pi)$
$c_{i,j}$	$(\pi, 3\pi/2)$
$d_{i,j}$	$(3\pi/2, 2\pi)$

Let us briefly recapitulate main ideas and basic properties of the used model [16] on which our treatment is based. Scattering matrix for individual contacts defines the transmission probability $|t|^2$ representing the overlap integral entering the standard tight-binding approach. The spin quantum number allows to distinguish energy bands and define anomalous Hall conductivity for each of the spin subsystems. For the sake of simplicity, the spin parts of wave functions will not be shown explicitly in the following treatment. We keep in mind that a typical AHE setting will entail two copies of the network with opposite spins and counter-propagating wave functions, i.e., ones composed of orbitals with opposite angular momentum.

Atomic orbitals on individual lattice sites $\vec{R}_{i,j}$ are modeled by rings of the radius R formed by one-dimensional conductors. Each electron subsystem (spin up and spin down) is represented by a one-way conductor. Their eigenenergies and eigenfunctions

$$E_m = \frac{\hbar^2 m^2}{2 m_0 R^2} \quad , \quad \psi_m(\phi) = \frac{1}{\sqrt{2\pi R}}\, e^{im\phi}, \tag{1}$$

where $\phi \in (0, 2\pi)$ is the polar angle are labeled by the quantum number $m = 0, \pm 1, \ldots$, which defines angular momentum. The assumption that electrons can orbit within rings in one direction only leads to a nonzero orbital momentum, and consequently removes the time reversal symmetry which is a necessary condition for the Hall effects to emerge.

In the square lattice shown in Fig. 1, each of the rings has four contact points with its neighbors which separate the domain of the wave function amplitude $A(\phi)\exp(i\delta\phi)$ into four sections listed in Table I. These allows to define four complex amplitudes a, b, c, d per lattice site fully determining the wave function for given δ.

Considering the positive orbital momenta of the atomic-type orbitals, $\delta > 0$, the amplitudes are controlled by the following relations:

$$\begin{aligned} e^{-i\delta\pi}\, a_{i,j} &= r\, e^{i\delta\pi}\, d_{i,j} + t\, b_{i+1,j}, \\ b_{i,j} &= r\, a_{i,j} + t\, e^{i\delta\pi}\, c_{i,j+1}, \\ c_{i,j} &= r\, b_{i,j} + t\, e^{i\delta\pi}\, d_{i-1,j}, \\ d_{i,j} &= r\, c_{i,j} + t\, e^{-i\delta\pi}\, a_{i,j-1}, \end{aligned} \tag{2}$$

where t denotes transition coefficient of the wave entering adjacent orbital while r represents part of the wave continuing the orbital motion. For the considered δ-type coupling, they are of the following general form [21]

$$t = \frac{i\alpha}{1 - i\alpha} \quad , \quad r = \frac{1}{1 - i\alpha} \quad , \quad |r|^2 + |t|^2 = 1, \tag{3}$$

where α is a real parameter, which is supposed to be an energy independent constant for the sake of the simplicity.

For infinite periodic network, the wave functions are of the Bloch form

$$|m, \vec{k}\rangle \equiv \Psi_{m,\vec{k}}(\vec{r}) = \frac{e^{i\theta_m(\vec{k})}}{\sqrt{N}} \sum_{i,j=1}^{N} e^{i\vec{k}\vec{R}_{i,j}} \sqrt{\frac{1}{2\pi R}}$$

$$\times A_{m,\vec{k}}(\phi)\, e^{i\delta_{\vec{k}}\phi}\, \delta(|\vec{r} - \vec{R}_{i,j}| - R) \equiv e^{i\vec{k}\vec{r}}\, u_{m,\vec{k}}(\vec{r}), \tag{4}$$

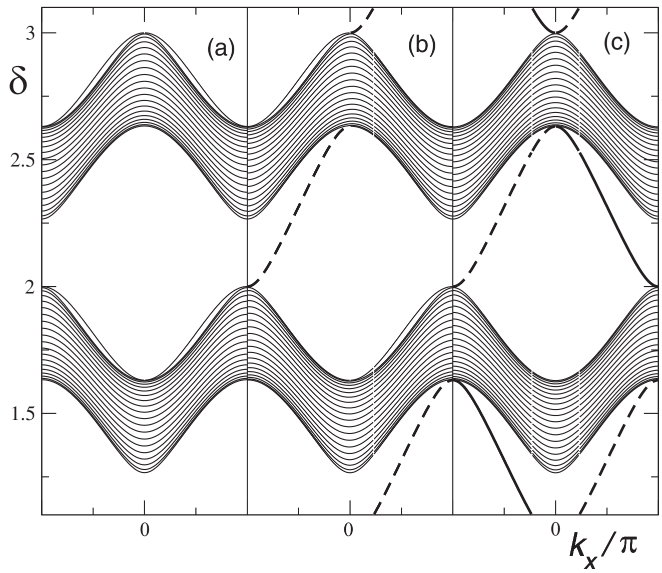

FIG. 2. Energy branches for a stripe subjected to different boundary conditions, $N = 20$, $|t|^2 = 0.3$, and $\alpha > 0$. Thick full and dashed lines represent edge states at lower and upper stripe edges, respectively.

where m and $\vec{k}$ are the band number and the wave vector, respectively, $\theta_m(\vec{k})$ denotes the Berry phase [25] and $u_{m,\vec{k}}(\vec{r})$ stands for the periodic part of Bloch functions. Wave function amplitudes $A_{m,\vec{k}}(\phi)$ are subject to the following Bloch conditions:

$$\begin{array}{llll} c_{i,j+1} = e^{ik_y}\, c_{i,j} & , & a_{i,j-1} = e^{-ik_y}\, a_{i,j}, \\ b_{i+1,j} = e^{ik_x}\, b_{i,j} & , & d_{i-1,j} = e^{-ik_x}\, d_{i,j}, \end{array} \tag{5}$$

where the wave vector components $k_{x,y}$ range from $-\pi$ to π pursuant to the choice of units, lattice constant $a_0 = 1$. Zero determinant of the resulting equations for wave function amplitudes yields the spectral condition for dimensionless parameter $\delta_{\vec{k}}$

$$\cos k_x + \cos k_y = -2\,\cos \delta_{\vec{k}}\pi - \frac{1-\alpha^2}{\alpha}\,\sin \delta_{\vec{k}}\pi, \tag{6}$$

which can be transformed into dispersion relation for eigenenergies using

$$E_{\vec{k}} = \frac{2\hbar^2 \delta_{\vec{k}}^2}{m_0} \tag{7}$$

in analogy to (1). This implicit expression for energy $E_{\vec{k}}$ corresponds to the kinetic energy of wave function (4).

For any energy-independent value of the parameter α, the spectrum comprises a series of nonoverlapping bands linked to states having orbital number m. Dispersions of the dimensionless parameter $\delta \sim \sqrt{E}$ are periodic with the period 2. Change of δ by one gives the same dispersion but shifted in $\vec{k}$ space by $\Delta\vec{k} = (\pi, \pi)$. All these features can be seen in spectrum obtained for a stripe samples shown in Fig. 2. Energy gaps become closed for $|t|^2$ approaching the value $|t|^2 = 0.5$ ($\alpha = \pm 1$) at which the bandwidth equals to that defined by $\Delta\delta = 1$. Fixed-energy contours (see Fig. 2 in Ref. [16]) are identical to the case of cosine band dispersion produced by the well-known square-lattice tight-binding model but energy scaling (7) is different.

In most real-world systems, the coupling between adjacent atomic orbitals is weaker than that to the atomic core and crystal formation lowers energy of electron states. For these reasons $|t|^2 < 0.5$ and $\alpha > 0$ satisfying the above requirements will be preferred in the following treatment. For $|t|^2 > 0.5$, electrons "orbit the stars" rather than the circular orbitals around $\vec{R}_{i,j}$, i.e., they are pushed into the interstitial positions. In these cases, the coupling gives rise to energy of electron states. For $|t|^2 = 1 - |r|^2 = 0$ and 1, the limit of isolated orbitals is achieved whereupon the dispersions reduce to flat bands.

III. EDGE STATES

Quantization of the anomalous Hall conductivity has also been observed on systems endowed with nonzero orbital momentum [26–28]. Generally it is attributed to the existence of chiral edge states within gap regions, i.e., states having opposite velocity at opposite sample edges. The existence of such states has been first predicted for two-dimensional systems subjected to a strong external magnetic field. In this case, there are two scaling areas, the area per unit magnetic flux A_ϕ and the unit cell area A_0. For rational values of A_0/A_ϕ, the eigenfunctions are of the Bloch form but the corresponding translation symmetry differs from that at zero magnetic field. As it has been shown by Thouless *et al.* [20] number of chiral edge states, Chern number, is fully determined by eigenfunction properties at the Brillouin zone boundary. The external magnetic field induces orbital momentum of atomic type states leading to an increase of the system energy. Chiral edge states are induced to minimize it. For this reason, they are insensitive to the boundary conditions at the sample edges [29]. These general arguments are not applicable in the zero field limit. Using a two-dimensional network model, the decisive role of boundary conditions for the existence of chiral edge states will be shown.

A stripe open along the $\hat{x}$ direction parallel to main crystallographic axis will be considered. Bloch conditions in the $\hat{x}$ direction, $b_{i+1,j} = e^{ik_x}\, b_{i,j}$ and $d_{i-1,j} = e^{-ik_x}\, d_{i,j}$, inserted into the basic equation set (2) give

$$\begin{array}{rcl} -e^{-i\delta\pi}\, a_{i,j} + t\, e^{ik_x}\, b_{i,j} + r\, e^{i\delta\pi}\, d_{i,j} & = & 0, \\ r\, e^{-i\delta\pi}\, a_{i,j} - e^{-i\delta\pi}\, b_{i,j} + t\, c_{i,j+1} & = & 0, \\ r\, e^{-i\delta\pi}\, b_{i,j} - e^{-i\delta\pi}\, c_{i,j} + t\, e^{-ik_x}\, d_{i,j} & = & 0, \\ t\, a_{i,j-1} + r\, e^{i\delta\pi}\, c_{i,j} - e^{i\delta\pi}\, d_{i,j} & = & 0. \end{array} \tag{8}$$

For a given k_x, the eigenvalue problem reduces to the problem for a single column of orbitals. It is independent of its position defined by the index i. Two types of boundary conditions in the $\hat{y}$ direction will be considered: (i) hard walls leaving circular orbitals untouched and (ii) those which cut orbitals in half as shown in Fig. 1 by dashed lines. Electrons are thus skimming or skipping along stripe walls.

Branch dispersions representing the case (i) for the column composed of $N = 20$ circular orbitals controlled by the boundary conditions $b_{i,N} = a_{i,N}$ and $d_{i,1} = c_{i,1}$ are shown in Fig. 2(a). At any band energy, the electron path at the upper edge ($\cdots \to a_{i,N} \to b_{i,N} \to a_{i-1,N} \to \cdots$) and that at the lower edge ($\cdots \to c_{i,1} \to d_{i,1} \to c_{i+1,1} \to \cdots$) carry skimming electrons in opposite directions, see Fig. 1.

As for case (ii), chiral edge states crossing the energy gaps appear. For stripe of the width Na_0, the boundary conditions $e^{i\delta\pi} d_{i,N+1} = c_{i+1,N+1} = e^{ik_x} c_{i,N+1}$ and $e^{i\delta\pi} b_{i,1} = a_{i-1,1} = e^{-ik_x} a_{i,1}$ correspond to hard walls cutting the orbitals in half on both sides of the sample. Resulting branch dispersions are shown in Fig. 2(c) for $N = 20$. In real space, electrons at edge current paths are skipping along stripe walls flowing in opposite directions compared to the previous case of skimming electrons.

There exists a peculiar possibility of imposing mixed boundary conditions, type (i)/(ii) at the lower/upper edge, giving rise to energy dispersions shown in Fig. 2(b). In this case, the symmetry leading to the presence of chiral edge states is lost and for chemical potential within the gap region the current flow is allowed only along one edge. It represents an ideal diode. Comparison of all three cases suggests that edge states are exclusively determined by boundary conditions. This conclusion is supported by a close connection of the anomalous Hall effect to the polarization which is known to be affected by boundary conditions. Opposite to the case of external magnetic fields (corresponding to rational values of A_0/A_ϕ), the appearance of chiral edge states is not determined by the Chern number which in our case has zero value. Necessary conditions for their appearance are the chiral symmetry of the current distribution across the stripe, i.e., oscillating currents are surrounded by current paths at the stripe edges leading currents in opposite direction, and relevant boundary conditions.

Note that for transition probability $|t|^2 > 0.5$ edge states crossing energy gaps appear only at edges for which hard wall leaves circular orbitals untouched. Nevertheless general conclusions remain unchanged.

IV. ELECTRONIC TRANSPORT: SCATTERING MATRIX APPROACH

Corbino disk samples can be used to measure conductivity components directly, at least in principle. In the limit of the infinite disk radius, it is equivalent to a stripe open in one direction (in our case $\hat{x}$) coinciding with a main crystallographic axis. A voltage drop applied to the opposite stripe edges induces current which has two components, perpendicular and parallel with the edges representing longitudinal (i.e., along $\hat{y}$) and Hall currents, respectively. Scattering matrix approach [18,30] will be used to evaluate corresponding conductivities, σ_{yy} and σ_{xy}, for the already described two-dimensional network model. It represents response to the electron concentration gradient of the fully coherent system, i.e. no dissipation is allowed within stripe interior. Dissipation is supposed to take place at the source and drain only where electrons are subjected to the equilibration processes. Stripe width can thus be identified with the equilibration length λ_e. Electron wave functions are thereby also losing information about their phases and the coherence length λ_c thus coincides with the stripe width as well.

Stripe interior is composed of electron paths leading currents along positive or negative $\hat{x}$ direction. To analyze conductivity contributions within the stripe, it is natural to

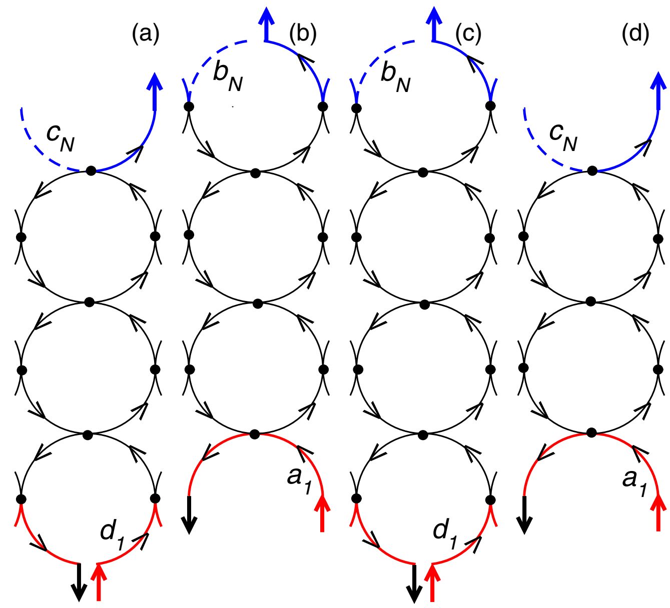

FIG. 3. Scheme of four possible boundary conditions applied to a single column. Source and drain are marked in red and blue, respectively.

choose one of the electron paths as the source and another as the drain, shown in figures by red and blue lines, respectively. Among the four possibilities sketched in Fig. 3, there are two qualitatively distinct cases. Source and drain paths can be chosen to carry current along the same direction (we choose to call it the Born-von Kármán case) or their currents have opposite direction (the chiral case). These two cases will be treated separately in following sections and the Hall conductivity of very clean but not fully coherent systems will be discussed in the last section.

Bloch conditions along $\hat{x}$ direction reduce problem to scattering within the single column of orbitals for each of the wave numbers k_x. Wave function amplitudes are defined by Eq. (8) accompanied by appropriate current currying conditions. Averaging over k_x gives relevant results. To get smooth enough dependence on the parameter δ defining the energy a large number of k_x values has to be used. Usually 10^4–10^5 k_x values uniformly spread through the interval $k_x \epsilon (-\pi, \pi)$ are considered. Results of the scattering matrix approach do not depend on the column position (i.e., index i) and unless necessary, this index will be skipped for brevity. For the presented numerical examples, unless explicitly stated, the model parameters $\alpha > 0$ and $|t|^2 = 0.3$ will be considered.

A. Born-von Kármán cases

Let us first consider source and drain paths at which electron velocity along $\hat{x}$ direction is positive, as sketched in Fig. 3(a). Electrons are supposed to be injected into strip region via the lower path, $d_1 = 1$, while they are absorbed by upper path and the condition $c_N = 0$ ensures zero injection from this side. Equation set (8) together with these conditions define uniquely all amplitudes within the column. Transition coefficient for given k_x is given by the amplitude $d_N(k_x, \delta)$. Total transition probability $T(\delta)$ defining current flow through

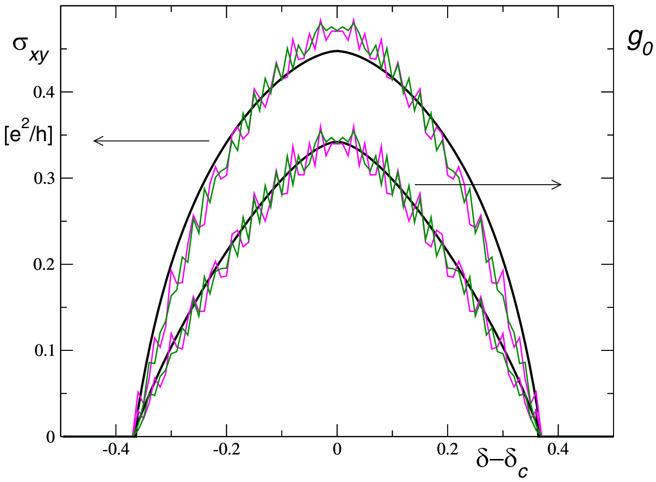

FIG. 4. Conductance $g_0(\delta)$ and anomalous Hall conductivity $\sigma_{xy}(\delta)$ obtained by using scattering matrix approach in the Born-von Kármán case. Magenta and green curves correspond to the column lengths $N = 15$, 25 and $|t|^2 = 0.3$. Smooth thick lines are Kubo formula results for unbounded systems.

a single column along $\hat{y}$ direction reads

$$T(\delta) \equiv \frac{h}{e^2}\, g_0(\delta) = \langle |d_N(k_x,\delta)|^2 \rangle_{k_x}, \tag{9}$$

where $g_0(\delta)$ stands for conductance per single column. In this case, transitions between orbitals are independent on their position. Except for fluctuations due to the size quantization it is independent of the considered column length $(N - 1/2)a_0$ as the green and magenta curves in Fig. 4 show. Considering an energy independent relaxation time represented by the parameter γ, the Kubo formula for longitudinal conductivity $\sigma_0(\delta)$ given by Eq. (A9) can formally be fit to approximate $g_0(\delta)$, as shown in Fig 4.

Current flow along $\hat{x}$ direction representing Hall current is not uniformly spread through the sample cross-section indicating the decisive role of wave function phases. Hall conductivity can be defined as follows:

$$\sigma_{\rm AH} \equiv \sigma_{xy}(\delta) = \frac{e^2}{h} \sum_{j=1}^{N} \langle |d_j(k_x,\delta)|^2 - |a_j(k_x,\delta)|^2 \rangle_{k_x}$$
$$\approx \sigma_{xy}^{\rm (int)}(\delta), \tag{10}$$

where the sum over j defines current into the right hand side column through coupling points enhanced by the current within drain path defined by setting $a_N(k_x,\delta) = 0$. Drain contribution decreases with rising column length and currents through coupling points becomes dominant. Again, except for the size quantization effect, the obtained results are independent on the column length and they are close to the intrinsic Hall conductivity $\sigma_{xy}^{\rm (int)}(\delta)$ given by Eq. (A8), as shown in Fig. 4. This comparison entails no fitting procedure. Note that conductance $g_0(\delta)$ defines the current through the unit cell cross-section and corresponding density is thus much larger than the Hall current density.

Another possibility is to choose source and drain paths leading electrons along negative direction as shown in Fig. 3(b). In this case ($a_1 = 1$ and $b_N = 0$), the conductance $g_0(\delta)$ defined by probabilities $|a_N(k_x,\delta)|^2$ coincides with that determined in the previous case. To obtain Hall conductivity instead of the drain path contribution the current of the source path has to be added by setting $d_1(k_x,\delta) = 0$. In this case, Eq. (10) gives for energy gap regions quantum value $-e^2/h$. This edge state effect has to be subtracted to obtain Hall conductivity within the bulk. Resulting δ dependence then coincides with that of the previous case.

B. Chiral cases

Transport between source and drain electron paths which carry current in opposite directions leads to qualitatively different results. Considering columns of length Na_0, the relevant conditions are $d_1 = 1$ and $b_N = 0$ or $a_1 = 1$ and $c_N = 0$, as sketched in Figs. 3(c) and 3(d), respectively.

Except for fluctuations caused by size quantization, the transition probability in both cases is once more independent of the column length. Compared to the Born-von Kármán case, conductance g_0 per single column is β-times smaller. This ratio is only weakly $|t|$-dependent, for example, for $|t|^2 = 0.3$ and $|t|^2 = 0.2$ the ratio β equals to 0.83 and 0.87, respectively.

Essential difference from the Born-von Kármán case is the dependence of the Hall conductivity on the distance between source and drain $N_s a_0$, which reads

$$\sigma_{xy}^{(\pm{\rm Ch})}(\delta) = \left\langle \sigma_{xy}^{\rm (Ch)}(\delta) \right\rangle \pm N_s \sigma_{xy}^{\rm (qf)}(\delta)$$
$$\equiv \left\langle \sigma_{xy}^{\rm (Ch)}(\delta) \right\rangle \pm \Delta\sigma_{xy}^{\rm (Ch)}(\delta), \tag{11}$$

where

$$\left\langle \sigma_{xy}^{\rm (Ch)}(\delta) \right\rangle \approx \beta\, \sigma_{xy}^{\rm (int)}(\delta) \tag{12}$$

denotes the average value of both chiral cases, (c) and (d). Plus and minus sign correspond to scattering problems with opposite chirality of current paths as sketched in the inset of Fig. 5. It is determined by velocity sign of electrons within the path attached to the source path. Contribution per unit cell $\sigma_{xy}^{\rm (qf)}(\delta)$ represents average friction between the nearest current paths. For large enough N_s it reaches a constant value as illustrated in Fig. 5.

The ratio β for the intrinsic part $\langle \sigma_{xy}^{\rm (Ch)}(\delta) \rangle$ turns out to be the same as for the longitudinal conductance. Its deviation of from one is the result of wave interference modified by the change of the boundary conditions.

Hall current enhancement $\Delta\sigma_{xy}^{\rm (Ch)}(\delta)$ entering Eq. (11) can be understood using the analogy with the viscous flow in classical fluids. The largest current is flowing via the path attached to source. It is stirring currents within adjacent stripe paths forcing them to move along the same direction. It explains the origin of the enhanced Hall current and in particular, its direction. In the fully coherent systems, the friction between current paths is determined not only by average coupling $|t|^2$ but it is modified by the wave interference which determines coupling between distant current paths.

C. Anomalous Hall effect in high conductivity region

Let us first discuss Hall conductivity within a coherent area of infinite systems. It has been found that the conductance $g_0(\delta)$ between paths leading current in opposite directions

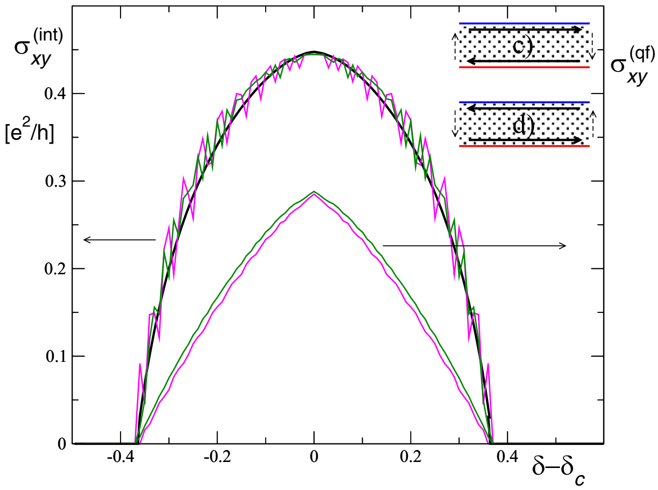

FIG. 5. Anomalous Hall conductivity contributions $\langle\sigma_{xy}^{(\mathrm{Ch})}(\delta)\rangle/\beta$ and $\sigma_{xy}^{(\mathrm{qf})}(\delta)/\beta$ obtained by using scattering matrix approach with chiral type boundary conditions. The two chiral scenarios are sketched in the inset whereas the letters refer to situations shown in Fig. 3. Magenta and green curves correspond to $N = 15,\ 25$, scaling factor $\beta = 0.83$ is discussed in the text and $|t|^2 = 0.3$. Smooth thick line is the Kubo formula result.

[chiral cases (c) and (d) in Fig. 3] is smaller than that for which they are flowing along the same direction [Born-von Kármán cases (a) and (b) in the same figure]. The occupation of neighboring paths leading current in opposite directions, has to be appropriately modified to unify both current densities. This polarization accompanying anomalous Hall effect allows electron transfer without enforced dissipation due to the current differences. It also ensures that intrinsic parts of the Hall conductivity is the same in both cases. Resulting Hall conductivity is given by average value of all four contributions discussed in previous two sections. They are of the same probability to appear and consequently sum of friction contributions depending on the column length is averaged out. Resulting anomalous Hall conductivity approaches intrinsic values given by the Kubo formula.

Different results are obtained for stripe samples shown in Fig. 1 with two types of boundary conditions discussed in the previous Sec. III as (i) and (ii) cases. They are composed of columns containing integer number of unit cells. In these cases, the edge electron paths carry current in opposite directions. Let us assume that attached source and drain prepared from the same material are coherently coupled to the stripe electron system which corresponds to scattering problems shown in Figs. 3(c) and 3(d). In the fully coherent case the Hall current enhancement defined by Eq. (11) is proportional to the stripe width $N_s a_0$ which for large enough N_s dominates.

Because of equilibration processes within source and drain, electrons are losing all information about their past. The stripe width $N_s a_0$ can be thus identified with the equilibration length λ_e. Longitudinal conductivity $\sigma_0 \equiv \sigma_{yy}$ can be approximated by the conductance per square area $N_s^2 a_0^2$, $\sigma_0 = N_s g_0$, and the Hall conductivity enhancement defined by Eq. (11) increases with σ_0 as observed in the high conductivity region.

Classical analogy of this effect is Couette flow observed in fluids placed between two plates. Motion of one plate induces fluid flow along the same direction which in the stationary case decreases linearly towards fixed one. In our case, the role of the moving plate is played by the current path attached to the electron source.

Dissipation processes are minimizing deviation from the equilibrium. They are thus trying to suppress enhanced Hall current by electron transitions into paths leading current in opposite direction. For strong enough dissipation, it can be thus expected that quantum friction contributions will be averaged out giving rise to intrinsic values of the Hall conductivity. Since current enhancement originates in wave interference even low angle inelastic scattering can be quite effective. It can be expected that corresponding relaxation time τ_{qf} could be much smaller than $\tau_e \propto \lambda_e$ which controls the longitudinal conductivity. Contrary to the case of unbounded systems the effect of transitions between chiral paths giving rise to opposite directions of the Hall current enhancements cannot be averaged out since for considered stripes their numbers differ by one. For corresponding current contribution, Eq. (11) can be used with $a_0 N_s$ replaced by the coherence length $\lambda_c \propto \tau_{qf}$. Anomalous Hall conductivity measured on a stripe of width w is thus given by averaged current density and we get

$$\sigma_{xy}^{(\pm\mathrm{Ch})}(\delta) \approx \sigma_{xy}^{(\mathrm{int})}(\delta) \pm \sigma_{xy}^{(\mathrm{qf})}(\delta)\,\frac{\lambda_c}{w}, \tag{13}$$

where plus and minus sign correspond to boundary conditions for which electrons are skimming or skipping along strip edges, respectively. Note that for $|t|^2 > 0.5$, the Hall conductivity has opposite sign but its general features remain unchanged.

Estimation of the measured Hall conductivity given by Eq. (13) has to be viewed as a rough approximation based on the assumption that the enhanced current distribution is spread uniformly through width w. If it becomes concentrated within a slab of the width w_{qf} at the edge vicinity the measured σ_{xy} becomes affected by the ratio w_{qf}/w. This problem desires a more advanced theoretical description based, for example, on the application of nonequilibrium Green's functions [31] employed in finite size systems.

Note that analyzed Hall currents are spin polarized. For negative values of δ, the orbital momentum and the Hall conductivity change their sign. Consequently, the spin polarization of Hall currents is changed as well.

V. TWO-BAND MODEL

As already mentioned in the introduction three regions of the anomalous Hall conductivity σ_{AH} in dependence on the disorder strength represented by the longitudinal conductivity σ_0 can be identified [1]. Scaling $\sigma_{\mathrm{AH}} \propto \sigma_0^{\nu}$ in the dirty-metal region with $\nu \approx 1.6$ has received considerable attention for σ_0 down below units of inverse $\Omega\,\mathrm{cm}$ [2,32,33]. Phonon assisted hopping between impurity localized states [34] gives the observed scaling. Empirically, there appears a transition from $\sigma_{\mathrm{AH}} \propto \sigma_0^{\nu}$ to the intrinsic region, $\sigma_{\mathrm{AH}} \sim$ const., for σ_0 between 10^3 and 10^4 inverse $\Omega\,\mathrm{cm}$ [7]. It is attributed to suppression of the band overlaps with decreasing disorder strength [35,36]. Calculations of intrinsic σ_{AH} values for inter-

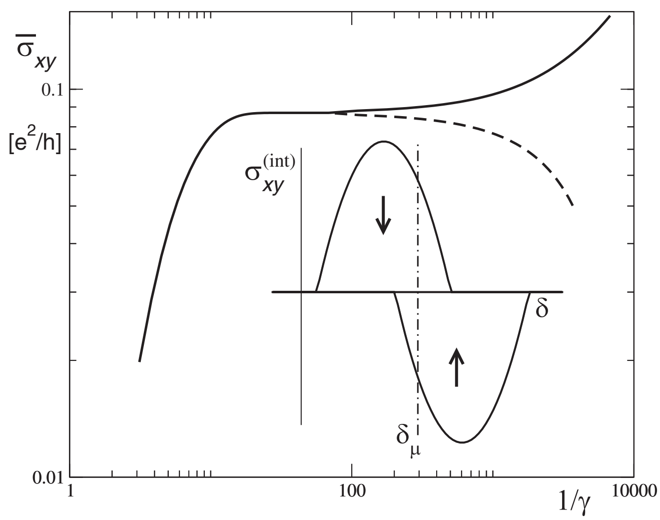

FIG. 6. Anomalous Hall conductivity for two band model as function of the disorder strength represented by the parameter γ ($|t|^2 = 0.3$). Recall that $\sigma_{xx} \propto 1/\gamma$ and width of the unperturbed band is taken as its unit. Sketch in the inset shows δ dependence of the intrinsic $\sigma_{xy}^{(\mathrm{int})}$ of both bands.

mediate σ_0 (often in terms of Berry curvature) are a popular topic for *ab initio* studies of ideal crystal structures [37–45] and even alloys [46,47] have been considered. While there is abundance of experimental data for systems falling into these two categories, data for high conductivity regions for which conductivity is well above 10^5 $(\Omega\,\mathrm{cm})^{-1}$ are scarce [2,48–51,53]. They require crystal structures with minimum lattice imperfections and low temperatures to suppress dynamical disorder due to the electron scattering with phonons and magnons. Outstanding bulk samples of iron [48] with σ_0 in excess of 10^8 $(\Omega\,\mathrm{cm})^{-1}$ showed an increase of σ_{AH} with σ_0, and the same was observed [49] for thin layers of somewhat lower quality. Newer study [2] confirms this and reports a decrease of σ_{AH} for cobalt rather than the increase seen in iron. This work shows almost constant σ_{AH} for nickel down to the lowest σ_0 achieved but better-conductivity samples [51] still show some increase in σ_{AH}.

To illustrate qualitative features of the measured anomalous Hall conductivity dependencies on disorder strength covering all three regions, the overlap of energy bands has to be taken into account. For the considered two-dimensional network model, two bands having opposite orbital momentum as well as spin orientation will only be considered for simplicity. Corresponding intrinsic Hall conductivities have opposite sign but their absolute values are supposed to be the same as shown in the inset of the Fig. 6. Their shift due to exchange interaction is approximated by a Zeeman splitting to obtain a nonzero Hall conductivity given by the sum of both band contributions

$$\bar{\sigma}_{xy}(\delta_\mu) = \langle \sigma_{xy}^{\downarrow}(\delta_\mu)\rangle_{\mathrm{av}} + \langle \sigma_{xy}^{\uparrow}(\delta_\mu)\rangle_{\mathrm{av}}. \qquad (14)$$

The effect of the disorder will be approximated by potential energy fluctuations. Assuming their Gauss distribution the ensemble averaging reads

$$\langle \sigma_{xy}^{\downarrow,\uparrow}(\delta_\mu)\rangle_{\mathrm{av}} = \frac{1}{\gamma\sqrt{2\pi}} \int e^{\frac{(\delta-\delta_\mu)^2}{2\gamma^2}} \sigma_{xy}^{\downarrow,\uparrow}(\delta)\, d\delta, \qquad (15)$$

where the dimensionless parameter $\gamma \sim \Gamma = \hbar/\tau_e$ in units of the unperturbed bandwidth, Eq. (A10), is assumed to be energy independent. Sum of both Hall conductivities decreases with increasing band overlap caused by the band broadening and for considered $|t|^2 = 0.3$ we find $\sigma_{xy} \propto \gamma^{-1.75}$ as shown in Fig. 6. Unperturbed band separation and Fermi level position are sketched in the inset. Within intrinsic region the effect of the band broadening vanishes.

The sum of quantum friction contributions of both bands, Eq. (13), multiplied by γ has been taken as a fitting parameter. The linear dependence of $\tau_{qf} \propto \lambda_c$ on a relaxation time $\tau_e \sim 1/\gamma$ representing longitudinal conductivity has been assumed through the whole range of disorder strength. It has been chosen to obtain the experimentally observed range of the intrinsic region covering approximately two orders of $\sigma_{xx} \propto 1/\gamma$ as presented in Fig. 6. This assumption is too simple to illustrate effect of quantum friction precisely. Like in the classical Couette flow, the friction desires some time to evolve. If it is much larger than the relaxation time τ_{qf} no effect can be expected. For this reason, the transition between intrinsic and high conductivity regions should be sharper.

Under conditions for which electrons are skimming along strip edges the friction contribution enhances Hall conductivity. They are expected to take place when electrons are orbiting close to atomic nuclei and are only tight-bounded to their neighbours. This is typical for d states (considering most transition metals, for example, the s states do not contribute to the AHE) and orbitals can only be slightly perturbed by the surface.

In exceptional cases [2], the Hall conductivity even changes its sign upon further decrease of the dissipation. Such a behavior can be explained within our analysis for electrons skipping along surfaces; the friction contribution has opposite sign and Hall conductivity decreases as shown in Fig. 6 by the dashed line. Skipping orbits appear if electron orbitals within bulk are of the radius larger than the interatomic distance of if they are orbiting around interstitial positions, i.e., $|t^2| > 0.5$ and this can occur in gapped materials [52]. Possibility that the coherence length of minority electrons within the upper band is larger than that within lower band cannot also be excluded as origin of this effect.

Despite of the model simplicity it gives qualitative features of scaling relations between anomalous Hall conductivity and longitudinal one. It is result of the competition between Hall currents of all overlapping bands. They are spin polarized and in high conductivity regions one of them dominates because of the quantum friction effect. Consequently the resulting Hall current becomes strongly spin polarized.

VI. SUMMARY AND CONCLUDING REMARKS

Existence of the quantum friction in fully coherent systems is the main message of our treatment [15]. The basic condition of its appearance is chirality of edge current paths within stripe samples. This effect persists even in not fully coherent systems for which the resulting Hall current enhancement is determined by the coherence length λ_c. This extrinsic contribution to the measured anomalous Hall conductivity due to the finite sample dimensions dominates in high conductivity regime. It represents a quantum analog of the classical Couette flow in fluids. It can be expected that it influences the observed spin Hall effect [53] in a similar way.

Presented view to the origin of the Hall current enhancement suggests that all scattering events affect all conductivity components but they do so with different efficiency. Electrons flowing along the voltage drop are subjected to dissipative processes which can be characterized by a relaxation time $\tau_e \propto \lambda_e$ determining longitudinal conductivity. On the other side, the enhanced Hall current decreases with disrupting the effective wave interference responsible for the coupling between current paths. Corresponding relaxation time $\tau_{qf} \propto \lambda_c$ can thus be substantially different from τ_e. Temperature-dependent inelastic scattering of electrons by phonons and magnons is destroying phase coherence but its effect to τ_e is weaker. This is consistent with existence of the intrinsic Hall conductivity plateau. Also an increase of the diffusion scattering of electrons at sample surfaces gives rise to the much larger suppression of τ_{qf} than τ_e as observed on high conductivity Ni samples [51]. Ratio of the electrical and thermal conductivity components has been studied for pure Fe samples [50] doped by Co and Si. In the limiting case of vanishing temperature where residual resistivity dominates, the validity of the Wiedemann-Franz law has been confirmed for ratios of diagonal as well off-diagonal components. It indicates that elastic scattering affects all components in a similar way and the much shorter τ_{qf} is proportional to τ_e. On the other side, a more complicated relation between both times can be expected for inelastic scattering. Unfortunately, there are not enough experimental data for full understanding of the electron transport in the high conductivity regions. Further detailed investigations of scattering effects in this regime are thus desired. A better understanding of the distribution of the enhanced Hall current across stripe and the possible dependence of the measured Hall conductivity on the sample width can help to map the evolution of the quantum friction effect in real systems.

Our analysis of quantum friction predicts that the increase of $\sigma_{\rm AH}$ (anomalous Hall conductivity) in the high-conductivity regime should be sensitive to the Hall bar width w. It is supported by experimental data for iron samples. Opposite to thin layers [2], an increase of $\sigma_{\rm AH}$ in massive crystals of comparable conductivity was not observed [48]. Nevertheless, more detailed measurements of the relationship between $\sigma_{\rm AH}$ and w are desirable to confirm our prediction and experimentally exclude skew scattering as the origin of $\sigma_{\rm AH}$ increasing in the high conductivity region. We stress that the investigation of relationship (13) calls for measurements on a set of devices spanning a large range of w.

Direction of the Hall current enhancement is controlled by the orientation of the current paths just touching strip edges which is determined by the boundary conditions. At least in cases for which suppression of the anomalous Hall effect is observed, the analysis of the current distribution at the sample edges is needed to verify origin of this effect. It would be ideal to be able to vary boundary conditions. If orbitals of magnetic impurities periodically distributed within nonmagnetic host lattice are of the radius larger than the distance between atoms this might be possible at least in principle. In these cases stripe edges can cut orbitals in half forcing electrons to skip or leave them untouched. Systems like Bi_2Te_3 family of topological insulators with univalent 3d magnetic ions [28] seem to be good candidates. In these systems skipping electrons are giving rise to chiral edge states crossing energy gap responsible for the observed quantum Hall effect. Creation of such systems with mixed boundary conditions might lead to new types of spintronic devices, diodes, allowing current flow along one direction only. In this case periodic distribution of ions is not necessary condition. Although this sounds as science fiction today we believe that technological progress will allow to realize such systems in the future.

ACKNOWLEDGMENTS

Authors thank V. Drchal and V. Špička for valuable comments, Y. Niimi for advice regarding experimental data, J. Kučera for technical support and head of the department J. J. Mareš for ensuring ideal working conditions for partly retired author P. Středa. We acknowledge financial support from 22-21974S (granted by the Czech Science Foundation) (GAČR).

APPENDIX: KUBO FORMULA RESULTS

Quantum theory of the linear response of unbounded systems to electric field at zero temperature leads, for diagonal conductivity components, to the well known Kubo-Greenwood formula [54]

$$\sigma_{ii}(\mu) = \pi e^2 \hbar \langle \, \mathrm{Tr}\{ v_i \delta(\mu - H) v_i \delta(\mu - H)\} \rangle_{\rm av}, \qquad \text{(A1)}$$

and for off-diagonal components the following expression derived by Bastin *et al.* [55]:

$$\sigma_{ij}(\mu) = i\hbar e^2 \times \int_{-\infty}^{\mu} \left\langle \mathrm{Tr} \left\{ \delta(\eta - H) \left[v_i \frac{dG^+}{d\eta} v_j - v_j \frac{dG^-}{d\eta} v_i \right] \right\} \right\rangle_{\rm av} d\eta, \qquad \text{(A2)}$$

where H denotes a single-electron Hamiltonian, v_i are components of the velocity operator and delta-function operator is defined as

$$\delta(\eta - H) = - \lim_{\epsilon \to 0^+} \frac{G^+(\eta) - G^-(\eta)}{2\pi i}, \qquad G^{\pm}(\eta) = \frac{1}{\eta - H \pm i\epsilon}. \qquad \text{(A3)}$$

For crystals with substitutional impurities the ensemble averaging $\langle \cdots \rangle_{\rm av}$ represents averaging over impurity configuration. Generally it is a complicated problem [56] which can be simplified by neglecting vertex corrections allowing to replace averaged product of resolvents $G(z)$ by product of their averaged operators

$$\langle G(z) \rangle_{\rm av} \equiv \frac{1}{z - H_{\rm eff}(z)}, \qquad \text{(A4)}$$

where z is the complex energy variable. It has the full crystal symmetry independently on the character of the scattering events, asymmetric scattering is not an exception. Effective

Hamiltonian $H_{\mathrm{eff}}(z)$ is non-Hermitian and energy dependent but it is analytic in both complex half-planes, $H_{\mathrm{eff}}(z^*) = H^+_{\mathrm{eff}}(z)$. Its standard form reads

$$H_{\mathrm{eff}}(z) = H_0 + \Sigma(z) \quad , \quad \Sigma(z) = \Delta(z) - i\Gamma(z), \qquad \text{(A5)}$$

where $H_0 = \langle H\rangle_{\mathrm{av}}$ represents virtual crystal and $\Sigma(z)$ is the energy-dependent self-energy determined by the coherent potential approach [57], as the best known theory to estimate effect of alloying.

The inverse value of its imaginary part represents a finite electron life-time τ. Note that matrix elements of $\Sigma(z)$ are diagonal in representation given by eigenfunctions of the Hamiltonian H_0. Using this representation and neglecting $\Gamma(\eta)$ entering one of the δ operators in Eq. (A1), we get

$$\sigma_{ii}(\mu) = e^2\hbar \sum_{n,\vec{k}} \frac{|\langle n,\vec{k}|v_i|n,\vec{k}\rangle|^2}{\Gamma_{n,\vec{k}}(\mu)}\, \delta(E'_{n,\vec{k}}(\mu) - \mu), \qquad \text{(A6)}$$

where $E'_{n,\vec{k}}(\eta) = E^{(0)}_{n,\vec{k}} + \Delta_{n,\vec{k}}(\eta)$, n and $\vec{k}$ denotes band number and wave vector, respectively. This expression coincides with the solution of the Boltzmann equation for longitudinal conductivity.

Neglecting vertex corrections in Eq. (A2) for the Hall conductivity, using equality $dG(\eta)/d\eta = -G^2(\eta)$ and having in mind that velocity matrix elements are diagonal in $\vec{k}$ we get

$$\sigma_{ij}(\mu) = \frac{e^2\hbar}{\pi} \sum_{n,n'}^{n\neq n'} \sum_{\vec{k}} \int_{-\infty}^{\mu} \frac{\Gamma_{n,\vec{k}}(\eta)}{[\eta - E'_{n,\vec{k}}(\eta)]^2 + \Gamma^2_{n,\vec{k}}(\eta)} \times 2\,\mathrm{Im}\left\{ \frac{\langle n,\vec{k}|v_i|n',\vec{k}\rangle\langle n',\vec{k}|v_j|n,\vec{k}\rangle}{[\eta - E'_{n',\vec{k}}(\eta) + i\Gamma_{n',\vec{k}}(\eta)]^2} \right\} d\eta. \qquad \text{(A7)}$$

With decreasing impurity concentration Γ decreases as well and the dominant contributions are those for which η-values are close to $E'_{n,\vec{k}}(\eta)$. If there is no band overlap the energy difference $\eta - E'_{n',\vec{k}}(\eta) \approx E'_{n,\vec{k}}(\eta) - E'_{n',\vec{k}}(\eta)$ dominates the denominator value and $\Gamma_{n',\vec{k}}(\eta)$ can be neglected if it is much smaller than the energy difference. This approach thus excludes significant effect of the decreasing impurity concentration to the Hall conductivity. This conclusion is general since in the pure crystal limit vertex corrections are vanishing in principle. Note that in this limit Eq. (A7) gives finite values even in the case of the band overlap [38,42,44].

Evaluation of the anomalous Hall conductivity for the considered ideal network model ($\Gamma \to 0$) is straightforward since the energy spectrum is for given spin subsystem composed of nonoverlapping bands and we have

$$\sigma_{xy}(\mu) = e^2\hbar \sum_{m,m'}^{m\neq m'} \sum_{\vec{k}} f_0(E_{m,\vec{k}} - \mu) \times 2\mathrm{Im}\left\{ \frac{\langle m,\vec{k}|v_x|m',\vec{k}\rangle\langle m',\vec{k}|v_y|m,\vec{k}\rangle}{[E_{m,\vec{k}} - E_{m',\vec{k}}]^2} \right\}, \qquad \text{(A8)}$$

where $f_0(E-\mu)$ denotes Fermi-Dirac distribution. Eigenenergies $E_{m,\vec{k}}$ are functions of the dimensionless $\delta_{\vec{k}}$ defined by Eq. (7) and velocity operator does not include spin-orbit term because of the one-dimensional character of electron orbitals,

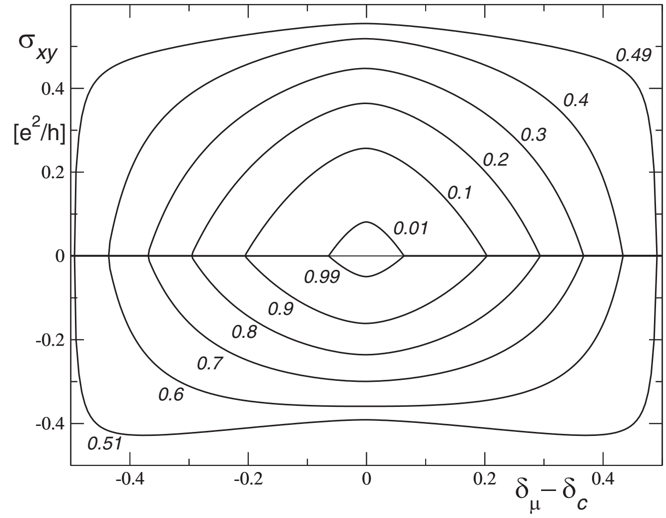

FIG. 7. Intrinsic anomalous Hall conductivity as function of the dimensionless parameter $\delta_\mu \sim \sqrt{\mu}$ for several values of $|t|^2$ ($\alpha > 0$).

$\vec{v} = -i\hbar\vec{\nabla}_{\vec{r}}/m_0$. Contributions for $m - m' = \pm 2$ vanish because periodicity of wave function amplitudes. The dominant contribution originates in elements with $m - m' = \pm 1$.

Assuming anticlockwise motion of electrons on circular orbitals ($\delta > 0$) the obtained anomalous Hall conductivities are shown in Fig. 7 for several values of the transition probability $|t|^2$. Note that their dependence on dimensionless parameter $\delta_\mu \sim \sqrt{\mu}$ is the same for all bands. Increase of $|t|^2$ above 0.5 changes sign of the orbital momentum since orbiting of electrons around interstitial positions becomes dominant. Their average radius is smaller than that for circular orbitals leading to smaller value of the orbital momentum. Except of the sign change the lower values of the Hall conductivity can thus be expected.

For opposite direction of the orbital motion, $\delta \to -\delta$, representing subsystem of the opposite spin orientation the anomalous Hall conductivity changes its sign. Resulting Hall conductivity is given by the sum of both subsystem conductivities and its nonzero value can thus only appear if the spin band degeneracy is removed.

To get longitudinal conductivity the simplest approach reducing effect of the disorder to an energy-dependent imaginary part $\Gamma(\mu)$ of the self-energy will be used

$$\sigma_0(\mu) = e^2\hbar \sum_{\vec{k}} \delta(E_{\vec{k}} - \mu)\, \frac{\Gamma(\mu)\,|v_x(\vec{k})|^2}{(E_{\vec{k}} - \mu)^2 + \Gamma^2(\mu)} = \frac{e^2}{h}\, \frac{1}{2\pi\gamma(\mu)} \oint_{F.S.} \left|\frac{d\delta_{\vec{k}}}{dk_x}\right|^2 \frac{dS_{\vec{k}}}{\sqrt{\left|\frac{d\delta_{\vec{k}}}{dk_x}\right|^2 + \left|\frac{d\delta_{\vec{k}}}{dk_y}\right|^2}}, \qquad \text{(A9)}$$

where dimensionless parameter $\gamma(\mu)$ relates to $\Gamma(\mu)$ as follows:

$$\Gamma(\mu) \equiv \frac{4\hbar^2\delta_\mu}{m_0}\, \gamma(\mu). \qquad \text{(A10)}$$

It has good physical meaning if its value is compared with the bandwidth represented by the range of available δ values.

[1] N. Nagaosa, J. Sinova, S. Onoda, A. H. MacDonald, and N. P. Ong, Rev. Mod. Phys. **82**, 1539 (2010).

[2] T. Miyasato, N. Abe, T. Fujii, A. Asamitsu, S. Onoda, Y. Onose, N. Nagaosa, and Y. Tokura, Phys. Rev. Lett. **99**, 086602 (2007).

[3] J. Smit, Physica **21**, 877 (1955); **24**, 39 (1958).

[4] J. M. Luttinger, Phys. Rev. **112**, 739 (1958).

[5] Y. Onose and Y. Tokura, Phys. Rev. B **73**, 174421 (2006).

[6] N. A. Sinitsyn, A. H. MacDonald, T. Jungwirth, V. K. Dugaev, and J. Sinova, Phys. Rev. B **75**, 045315 (2007).

[7] S. Onoda, N. Sugimoto, and N. Nagaosa, Phys. Rev. B **77**, 165103 (2008).

[8] H. Ishizuka and N. Nagaosa, Phys. Rev. B **96**, 165202 (2017).

[9] An explicit expression for this link (between orbital momentum and AHE) is Eq. (28) of Wang *et al.*, Phys. Rev. B 76, 094406 (2007) See also review by Yu. Mokrousov (Chapter 6 of Topology in Magnetism, Springer Series in Solid-State Sciences 192); time-reversal symmetry can be broken by spin-orbit, noncollinear magnetic order, etc.

[10] R. Shindou and N. Nagaosa, Phys. Rev. Lett. **87**, 116801 (2001).

[11] P. Středa and T. Jonckheere, Phys. Rev. B **82**, 113303 (2010).

[12] R. Karplus and J. M. Luttinger, Phys. Rev. **95**, 1154 (1954).

[13] E. N. Adams and E. I. Blount, J. Phys. Chem. Solids **10**, 286 (1959).

[14] R. C. Fivaz, Phys. Rev. **183**, 586 (1969).

[15] Term quantum friction is used also by other authors in a different context: Volokitin and Persson (Phys. Rev. Lett. **106**, 094502 (2011)) discuss van der Waals friction between graphene and an amorphous silicon dioxide substrate; Vignale and MacDonald (Phys. Rev. Lett. **76**, 2786 (1996)) consider drag in superfluid electron-hole condensates; hydrodynamic transport in electron liquids allows to introduce the concept of viscosity (Phys. Rev. B **96**, 195128 (2017)). In our case, we focus on quantum interference effects in the single-particle picture.

[16] P. Středa and J. Kučera, Phys. Rev. B **92**, 235152 (2015).

[17] G. Berkolaiko, P. Kuchment: *Introduction to Quantum Graphs*, Amer. Math. Soc., Providence, R. I., 2013.

[18] R. Landauer, IBM J. Res. Dev. **1**, 223 (1957); Philos. Mag. **21**, 863 (1970).

[19] K. von Klitzing, Rev. Mod. Phys. **58**, 519 (1986).

[20] D. J. Thouless, M. Kohmoto, M. P. Nightingale, and M. den Nijs, Phys. Rev. Lett. **49**, 405 (1982).

[21] P. Exner, J. Phys. A: Math. Gen. **29**, 87 (1996).

[22] J. T. Chalker and P. D. Coddington, J. Phys. C **21**, 2665 (1988).

[23] J. B. Marston, Phys. Rev. Lett. **82**, 4906 (1999).

[24] K. Kobayashi, T. Ohtsuki, H. Obuse, and K. Slevin, Phys. Rev. B **82**, 165301 (2010).

[25] D. Xiao, M.-C. Chang, and Q. Niu, Rev. Mod. Phys. **82**, 1959 (2010).

[26] B. A. Bernevig, T. L. Hughes, and S. C. Zhang, Science **314**, 1757 (2006).

[27] M. König, S. Wiedmann, Ch. Brüne, A. Roth, H. Buhmann, L. W. Molenkamp, X. L. Qi, and S. C. Zhang, Science **318**, 766 (2007).

[28] C.-Z. Chang, J. Zhan, Xiao Feng, J. Shen, Z. Zhan, M. Guo, K. Li, Y. Ou, P. Wei, L.-L. Wang, Z.-Q. Ji, Y. Feng, S. Ji, X. Chen, J. Jia, X. Dai, Z. Fang, S.-C. Zhang, K. He, Y. Wang, L. Lu, X.-C. Ma, and Q.-K. Xue, Science **340**, 167 (2013).

[29] P. Středa, J. Kučera, D. Pfannkuche, R. R. Gerhardts, and A. H. MacDonald, Phys. Rev. B **50**, 11955 (1994).

[30] M. Büttiker, Y. Imry, R. Landauer, and S. Pinhas, Phys. Rev. B **31**, 6207 (1985).

[31] A. A. Kovalev, K. Vyborny and J. Sinova, Phys. Rev. B **78**, 041305(R) (2008).

[32] A. Fernández-Pacheco, J. M. De Teresa, J. Orna, L. Morellon, P. A. Algarabel, J. A. Pardo, and M. R. Ibarra, Phys. Rev. B **77**, 100403(R) (2008).

[33] S. Sangiao, L. Morellon, G. Simon, J. M. De Teresa, J. A. Pardo, J. Arbiol, and M. R. Ibarra, Phys. Rev. B **79**, 014431 (2009).

[34] X.-J. Liu, X. Liu, and J. Sinova, Phys. Rev. B **84**, 165304 (2011).

[35] P. Středa, Phys. Rev. B **82**, 045115 (2010).

[36] T. Naito, D. S. Hirashima, and H. Kontani, Phys. Rev. B **81**, 195111 (2010).

[37] T. Jungwirth, Qian Niu, and A. H. MacDonald, Phys. Rev. Lett. **88**, 207208 (2002).

[38] Y. Yao, L. Kleinman, A. H. MacDonald, J. Sinova, T. Jungwirth, D.-s. Wang, E. Wang, and Q. Niu, Phys. Rev. Lett. **92**, 037204 (2004).

[39] H.-R. Fuh and G.-Y. Guo, Phys. Rev. B **84**, 144427 (2011).

[40] J.-C. Tung, H.-R. Fuh, and G.-Y. Guo, Phys. Rev. B **86**, 024435 (2012).

[41] D. Ködderitzsch, K. Chadova, J. Minár, and H. Ebert, New J. Phys. **15**, 053009 (2013).

[42] H. Chen, Q. Niu, and A. H. MacDonald, Phys. Rev. Lett. **112**, 017205 (2014).

[43] A. K. Nayak, J. Erika Fischer, Y. Sun, B. Yan, J. Karel, A. C. Komarek, C. Shekhar, N. Kumar, N. Schnelle, J. Kübler *et al.*, Sci. Adv. **2** (2016).

[44] K. Manna, L. Muechler, T.-H. Kao, R. Stinshoff, Y. Zhang, J. Gooth, N. Kumar, G. Kreiner, K. Koepernik, R. Car, J. Kübler, G. H. Fecher, C. Shekhar, Y. Sun, and C. Felser, Phys. Rev. X **8**, 041045 (2018).

[45] C. Helman, A. Camjayi, E. Islam, M. Akabori, L. Thevenard, C. Gourdon, and M. Tortarolo, Phys. Rev. B **103**, 134408 (2021).

[46] Y. Q. Zhang, N. Y. Sun, R. Shan, J. W. Zhang, S. M. Zhou, Z. Shi, and G. Y. Guo, J. Appl. Phys. **114**, 163714 (2013).

[47] I. Turek, J. Kudrnovsky, and V. Drchal, Phys. Rev. B **86**, 014405 (2012).

[48] A. K. Majumdar and L. Berger, Phys. Rev. B **7**, 4203 (1973).

[49] R. Schad, P. Belien, G. Verbanck, V. V. Moshchalkov, and Y. Bruynseraede, J. Phys.: Condens. Matter **10**, 6643 (1998).

[50] Y. Shiomi, Y. Onose, and Y. Tokura, Phys. Rev. B **79**, 100404(R) (2009).

[51] Epitaxial layers of nickel (reported in Phys. Rev. B **85**, 220403(R) (2012) by Xiaofeng Jin and co-workers) can be further improved by adding a copper layer on top of the device. While the cap increases the conductivity only moderately, larger coherence length due to specular reflection (rather than diffuse scattering in the former case) leads to the strong increase of

σ_{AH}, see Jianli Xu, Yufan Li, Dazhi Hou, Li Ye, and X. Jin, Appl. Phys. Lett. **102**, 162401 (2013).
[52] C. A. Corrêa and K. Vyborny, Phys. Rev. B **97**, 235111 (2018).
[53] Y. Omori, E. Sagasta, Y. Niimi, M. Gradhand, L. E. Hueso, F. Casanova, and Y. C. Otani, Phys. Rev. B **99**, 014403 (2019).
[54] D. A. Greenwood, Proc. Phys. Soc. **71**, 585 (1958).
[55] A. Bastin, C. Lewinner, O. Betbeder-Matibet, and P. Nozieres, J. Phys. Chem. Solids **32**, 1811 (1971).
[56] K. Levin, B. Velický, and H. Ehrenreich, Phys. Rev. B **2**, 1771 (1970).
[57] B. Velický, S. Kirkpatrick, and H. Ehrenreich, Phys. Rev. **175**, 747 (1968).